A THEORETICAL DESIGN MODEL USING THE SHAPE MEMORY ALLOY, NITINOL, IN A ROBOTIC FINGER

A Thesis

Presented to the faculty of the Department of Mechanical Engineering

California State University, Sacramento

Submitted in partial satisfaction of
the requirements for the degree of

MASTER OF SCIENCE

in

Mechanical Engineering

by

Jonathan Ryan Glover

FALL
2022

© 2022

Jonathan Ryan Glover

ALL RIGHTS RESERVED

A THEORETICAL DESIGN MODEL USING THE SHAPE MEMORY ALLOY, NITINOL, IN A ROBOTIC FINGER

A Thesis

by

Jonathan Ryan Glover

Approved by:

_____, Committee Chair
Dr. Kenneth Sprott

_____, Second Reader
Dr. Alan Meier

_____
Date

Student: Jonathan Ryan Glover

I certify that this student has met the requirements for format contained in the University format manual, and this thesis is suitable for electronic submission to the library and credit is to be awarded for the thesis.

_____, Department Chair _____

Dr. Troy Topping Date

Department of Mechanical Engineering

Abstract

of

A THEORETICAL DESIGN MODEL USING THE SHAPE MEMORY ALLOY, NITINOL, IN A ROBOTIC FINGER

by

Jonathan Ryan Glover

Currently, robotics and end-effectors pertaining to extremity functions, such as a hand or picker, their mechanical components have limitations, including servo motors, pulleys, hinges, and other components that drive a system of displacements. Each component in a dynamic system has an association of input-output lag or error from the control system to the point of physical movement that can cause delayed responses. In this work, a numerical model using shape memory alloys, (SMAs) as a solution architecture of a robotic finger to achieve faster response time near that of a natural human finger was performed. Nitinol was selected as the SMA material and simplified cantilever beam modeled in MATLAB Simulink to analyze electrothermal responses. The simulation results will show approximately 46% faster response time compared to a traditional

robotic system. This is a theoretical approach; furthermore, additional experimental research will need to be conducted for physical proof of concept.

_____, Committee Chair
Dr. Kenneth Sprott

_____
Date

ACKNOWLEDGEMENTS

First, I would like to thank our Lord and Savior Jesus Christ, for without him none of this would exist. I would like to acknowledge my professors that had advised and/or helped contribute their time and experience; Dr. Kenneth Sprott, Dr. Alan Meier, Dr. Troy Topping, Dr. Ilhan Tuzcu, and Dr. Akihiko Kumagai. This work is dedicated to my wife, Tiffany. Thank you for your wholehearted support in making this a reality. To our children Michelle and Cruz, you will carry on this legacy of curiosity to solve problems that inspire those around you. My mother Nancy and siblings; Rob, Rodney, Robin, Sarina, Brandon, my twin sister Jamie, and Matt, without you I wouldn't be here. To my family that has passed, my dad Robert, and brother Justin, you are always in my heart fueling the passion to never give up, because life is too short. I also would like to acknowledge that having a learning disability does not prevent you from having the ability to do great things!

TABLE OF CONTENTS

Page

LIST OF TABLES

Tables Page

LIST OF FIGURES

Figures Page

1. INTRODUCTION

1.1 Purpose

Robotics in biomechanical engineering have made significant innovative strides in surgical procedure rooms, manufacturing of medical devices, and prosthetic adaptation. Currently, robotics, and specifically the end-effectors pertaining to extremity functions, such as a hand or picker, have limitations in their mechanical components, including servo motors, pulleys, hinges, and other components that drive a system of displacements.[1] Each component in a dynamic system has an association of input-output lag or error-controlled systems that can cause delayed responses. Advancements in control board processing speeds have helped to reduce these lag input-output errors, but their physical delays still exist when applying a pulse response through these systems. These time delays can be accounted for if the end displacement, or range of the positioned window is defined. For the application of a robotic hand in prosthetics, the end displacement is an unknown variable since an individual needs to be able to have motor functions as a natural human hand would, i.e., simultaneous response through a neurological system, along with smoother movement to the muscular system. The proposed application of shape memory alloys (SMAs) in the form of a coupling push-pull system by way of thermoelectric actuation, will address limitations of traditional electric servo-motor-drive systems currently used in a robotic hand. A theorical model providing comparative analysis between the SMA hysteresis heat gradient control response and the robotic hand displacement response relative to that of a human hand controlled by a human nervous system, has been developed as proof of concept. The focus is on a single

extremity finger, restricted to one-dimensional reduction to simplify the model. The analysis developed can be multiplied into a full human hand analysis in future work. The material selection, workability, thermal gradient threshold and electrical properties have also been explored in the development of a theoretical modeled solution.

1.2 Material Background

The exhibitory on shape memory alloys (SMAs) effect was first discovered in the 1960's with a material's ability to "remember" their shape even after deformation. Unlike other metals once SMAs are deformed past the elastic region with an applied stress, they can reverse their mechanical behavior with introduction of heat. SMAs have been extensively researched for their heat driven phase transformation between martensite and austenite. Duerig *et al.* [2] illustrates the most fundamental property descriptors comparing traditional metals to SMAs with a focus on yield strength to stress rate, modulus to recovery stress, and ductility to martensite start temperature, M_s. SMA properties are a function of four external dependent parameters: temperature (T), stress (σ), strain (ε) and time (t). Shape memory alloys undergo shape change without volume being compromised unlike the martensite transformation in steel. Two mechanisms to produce a shape change without volume are slip (non-reversible) and twining (reversible). Twining introduces multiple directions in large variants of shear. For example, CuZnAl martensite has 4 variants and NiTi martensite displays 3 variants. [3], [4] The maximum ratio of martensite to austenite yield strength allows for deformation

recovery (typical ranging from 0.1 to 0.2). Research activity in this field has produced a nickel-titanium (Nitinol) family of binary alloys including; AgCd, AgZn, AuCd, CuAl, CuZn, FeBe, FePt, NbTi, NiAl, along with ternary alloys. The alloys developed provide a range of M_s temperatures between -273 and 100°C. [5], [6] The temperature versus strain hysteresis of NiTi and Cu-based alloys for their austenite-martensitic transformations are thermoelastic, Figure 1 illustrates a typical hysteresis loop and Figure 2 is a schematic that demonstrates the physical shape memory effect.

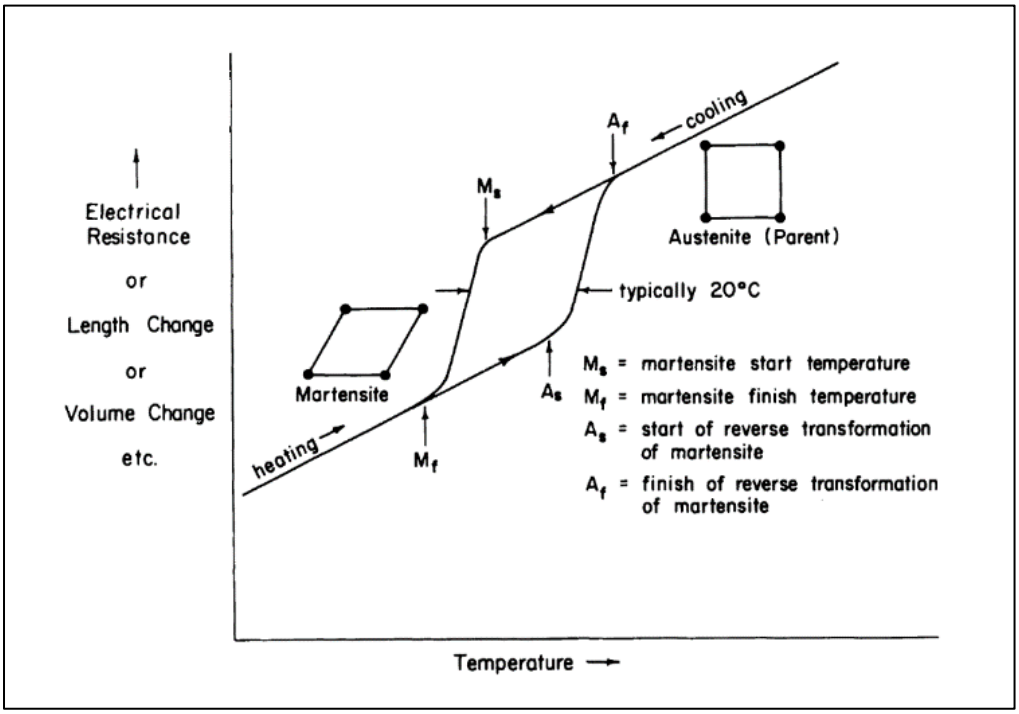

Figure 1: Hypothetical plot of property changes versus temperature for a martensitic transformation occurring in a shape memory alloy. The parent phase (austenite) is represented by the square lattice, which upon martensitic transformation is distorted in the rhombic product phase (martensite). Characteristic temperatures are defined in the inset. Reproduced from Duerig *et. al.* [2]

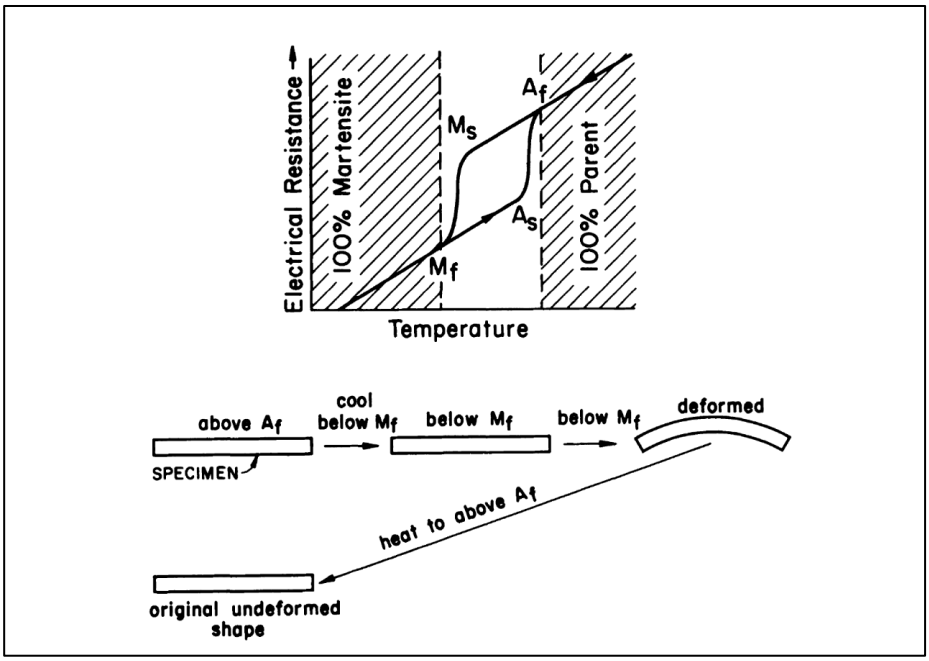

Figure 2: The shape memory effect is described with reference to a plot of electrical resistance vs temperature from which the characteristic transformation temperature M_s, M_f, A_s and A_f are determined. Reproduced from Duerig *et. al*. [2]

The hysteresis loop has been studied in several analyses due to the slight change in atomic weight structures impact on SMAs phase transformation characteristics. SMAs have a superlattice structure of body-centered cubic (BCC) with sublattices from the parent phase. [7] Figure 3 presents the Ni-Ti binary phase diagram which includes a percentage scale weight of titanium and the sublattice BCC referred to as β-phase alloying. Parent phases can change with different heat treatments and composition techniques called R-phase transitions, which determines SMA mechanical properties.

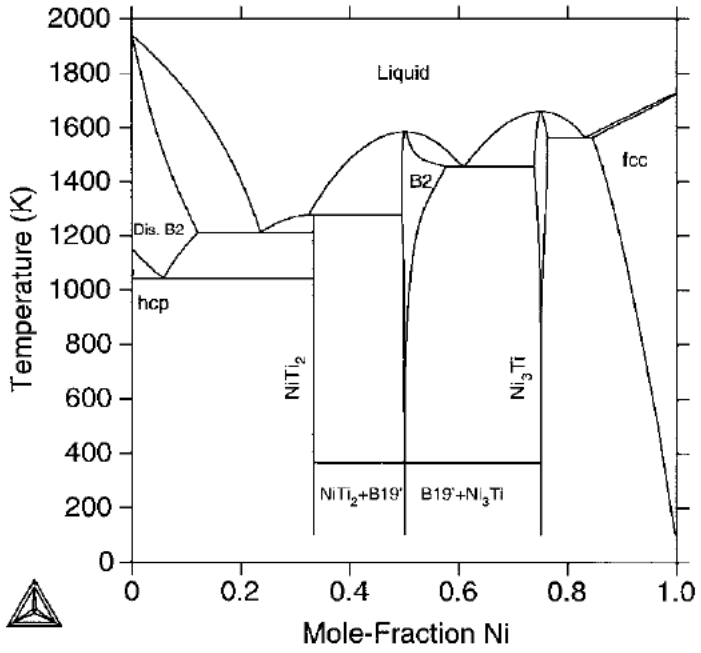

Figure 3: The Ni-Ti phase diagram calculated with the descriptions of B2 and B19' phases assessed in Tang *et. al's* work. Reproduce from Tang *et. al.* [7]

By way of illustration, for a specimen aging after solution-treatment, the critical stresses are low, but when the material is annealed after cold-working, the critical stresses are significantly higher. The proposed mechanisms for this behavior is that dislocations have a stronger effect on the mechanical properties associated with the R-phase transition.[2] These R-phase dislocations provide a mechanism for the storage of shape memory effect (SME) resulting in grain boundary twinning. The martensite twin lattice can shift and be replaced by its neighboring lattice, creating no volume change or detwinning during austinite transformation.

NiTi has been the most commercially used SMA due to the wide range of compositional stability, range of shape memory temperatures, large strain recovery, and advanced mechanical behavior when formed to a targeted β-phase such as super-elasticity and two-way SME. Frenzel *et. al.* [8] produced high-precision data on the phase transformation temperatures in NiTi, including numerical expressions for the effect of Ni on the M_S, M_F, A_S, A_F and T_0 temperatures. Clear experimental evidence was provided confirming the predictions of Tang *et al.* [7] regarding deviations from a linear relation between the thermodynamic equilibrium temperature single-step transformation and the Ni concentration. In addition to affecting the phase transition temperatures, increasing Ni contents were also observed to decrease the width of the thermal hysteresis loop and the heat of transformation.[8] A larger hysteresis loop can achieve longer life cycles and increase the fatigue life with only a slight increase mass percent of nickel.[9]–[12] For this reason, the selection of 50-55% mass Ni was chosen for evaluation in the current study.

A disadvantage of SMAs, is their latent heat loss on cooling and associated longer reverse transformation times, (i.e., from austenite to martensite). An addition of a third element, such as Cu, can narrow the hysteresis loop in the martensite two-step transformation, creating higher resistivity, lower load, and also an increase in fatigue cycle life.[2] Akgul *et al*, determined the effect of the cooling rate on the thermal and thermomechanical behavior of NiTiHf high-temperature shape memory alloy by differential scanning calorimetry (DSC) and via running isobaric thermal cycling experiments. It was concluded that the transformation temperatures and thermal hysteresis values do not depend on changes in the cooling rate. Their results also determined that the austenite to martensite transformation enthalpy, increased with an increase in the cooling rate. The recoverable strain values which were determined from isobaric thermal cycling experiments were constant since the transforming volume does not change with a change in cooling rate.[13]

1.3 Introduction to Robotic Hands

Prosthetic limbs have been a solution to amputees for centuries. The prosthetics limbs were originally produced from available mundane materials such as wood. As society evolved, so did the technologies in the advancements of materials towards prosthetics. In 2005, the Defense Advanced Research Project Agency (DARPA) backed a research project called “Revolutionizing Prosthetics,” that started a new era of prosthetics with a goal to improve the quality of life for upper limb amputees. Funding was granted to Deka Integrated Solutions Corp for their development of the Luke Arm, later called

DEKA arm after founder and American Inventor Dean Kamen. [14] [15] In 2014, the DEKA arm received FDA approval to be produced through both a VA health system and commercially as the LUKE Arm, manufactured by Mobius Bionics. More than 90 percent of patients that received a Gen2/3 DEKA arm users were able to perform new tasks that were previously not possible prior to receiving the new prosthetic. [16] The DEKA arm uses pre-programmed input controls operated by a combination of foot movement, pneumatic bladders, and myoelectrodes. The system has about 12 different dimensions of motion and consist of wire pulleys, motors, microcontrollers and sensors. Since the DEKA arm project, DARPA has launched a series of research projects with experiments designed with the goal of continuing to evolve upper limb prosthetics along with biomedical advances on invasive and non-invasive EMG sensors. Other global developments such as Pisa/IIT Softhand+[17], [18], Ottoback Michelangelo [19], and Dexter [20] use highly complex materials, gears, pulleys, servo motors, EMG sensors and other technical advances, to develop prosthetics with wide range of dimensional movements. A highly sophisticated anthropomorphic robotic hand produced by Xu and Todorov [21] has 10 Dynamixel servos to control hand extremities. Their experimental data, presented in Figures 4 and 5, displayed 20 repetitions within a span of approximately 45 seconds and had high displacements about the Z-axis. Furthermore, the frequencies in Figure 5 were extrapolated such that each interval was approximately 2.25 seconds and the X-Y direction movements demonstrated slight intermittent fluidity on the sinusoidal response.

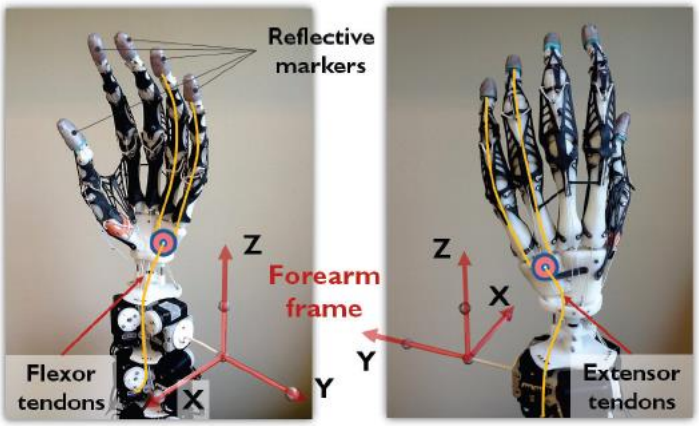

Figure 4: Image of anthropomorphic robotic hand, labeled pictures showing the differential pulley transmission for ring, little fingers, and reflective markers as coordinates with respect to forearm datum. Reproduced from Xu and Todorov. [21]

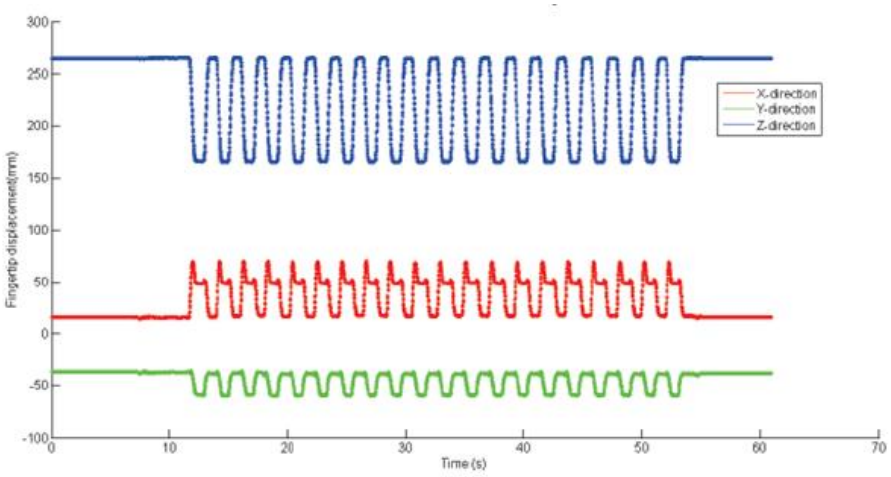

Figure 5: Frequency displacement results for the ring-fingertip during 20 repetitions of flexion and extension motions. Reproduced from Xu and Todorov. [21]

1.4 EMG Signal Background

Myoelectrodes (used in conducting electromyography, EMG) are used to obtain the myoelectric (ME) signals that humans' naturally produce. ME are electrical pulses from a humans nervous system that control extremity motor functions.[22] In amputees, although their extremities are no longer present, the brain still produces and processes these EMG signals as if they are still intact. Engineers and medical professionals have developed sensors that can trace, identify, and amplify these frequencies to widen the voltage response in control systems with respect to time. [23]–[25] EMG signals can be collected from an amputee's residual limb(s) and then used to control prosthetic extremities. Araki *et al*, illustrates that muscles associated with the middle finger motion produced EMG signals that were measured by electrodes, amplified (sensitivity was set to 0.1 mV/V) and bandpass filtered between 10~15 kHz with a bio-signal amplifier (AB-611J, product by Nihon Kohden), then recorded with a sampling frequency of 10 kHz. [26] They further defined 6 frequencies X1 to X6 histogram calculated from the surface EMG signal of a flexor muscle, and X1e(t) to X6e(t) are the joint angle extensor muscle at time, t. The joint angle, θ(t), is calculated with:

$$\theta(t) = \theta_0 + \sum_{i=1}^{6}\{a_i X_i^f(t) + b_i X_i^f(t)\} \qquad (1)$$

where θ_0, is the bias angle and a_i, b_i are weighted coefficients.

In recent years, the Michigan University Biomedical Engineering group lead by Vu *et. al.*, implemented targeted muscle reinnervation (TMR), an invasive device sensor that

increased multiple control signals by transferring the divided peripheral nerves in a residual limb to intact local or regional muscles. Their development is known as RPNI (regenerative peripheral nerve interface) [27], Figure 6 demonstrates the time classification of the EMG signal time to the movement of fingers with amplified voltage from RPNI. The real-time parameters from RPNI research, with respect to time correlation of EMG signals, can be utilized as the amplified input voltages to thermo-mechanically and accurately improve workability of SMA's time response. These time base signals of EMGs and the time base for a traditional robotic hand have been established as comparable data to the model development in this study.

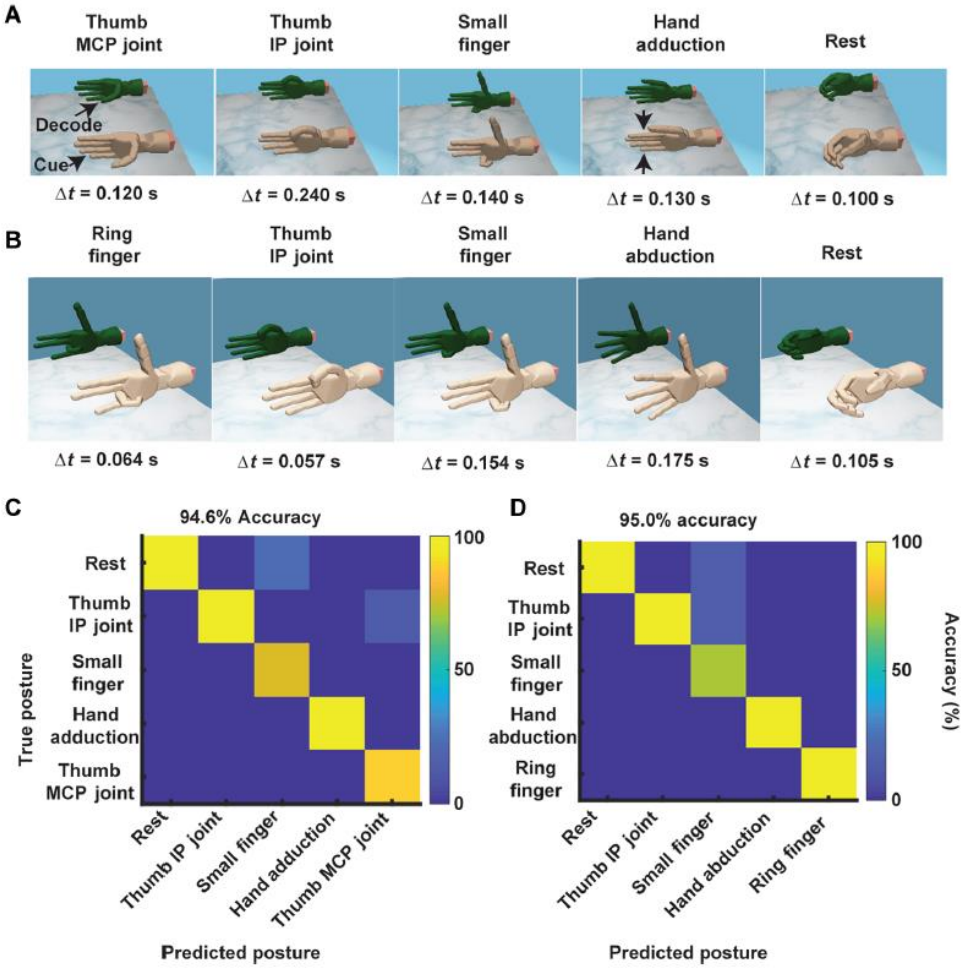

Figure 6: Real-time classification of finger movements. (**A** and **B**) P3 and P4's discrete control of thumb MCP joint (opposition), thumb IP joint (flexion), small finger, adduction, and rest for P3, and ring finger, thumb IP joint, small finger, abduction, and rest for P4. The fastest motion selection times are shown for each posture. (**C** and **D**) Offline confusion matrix of the postures used in (A) and (B), respectively. The *y* axis represents the true posture, whereas the *x* axis represents the predicted posture. The color map indicates the accuracy (%) of the classifier's prediction. Reproduced from Vu *et. al.* [27]

2. SMA CONTROL METHOD

2.1 Background

SMA applications can be divided into four actuator categories; free recovery, constrained recovery, super-elasticity, and work production.[2] The focus of the current study is on actuator work production, based on the geometry of a cantilever beam in bending. SMA actuators are still cumbersome in predicting an accurate hysteresis loop because of their inherent nonlinear functionality. A computational model is required to simulate an actuator and the development of constitutive laws have been utilized to obtain partial solutions that address the hysteresis loop derivation. In 1935, Ferenc Preisach, performed the initial analysis while uncovered the characteristics of the hysteresis loop in ferromagnetic materials.[28] A number of models that followed Preisach have included variations in the computational controls and the materials thermomechanical behavior. For example, Brinson *et al*. [29] developed a phenomenological model based on previous work by Tanaka *et al*. [30]. Tanaka's work successfully described classic SMA behavior. In their models, the transformation kinetic equations relating the martensite volume fraction to stress and temperature were described using cosine functions.[31] Brinson further analyzed the Preisach fundamental model with a focus on the strain volume fraction coefficient for both twinning and detwinning of the martensitic phase transformation. Following Brinson's work, Majima further refined their approach by tracking the control system based on the experimental bias actuator; the spring-mass-damper system.[31] The force function was

not defined in relation to thermal conductivity. In the model development for this study, modified equations are used in order to address the relationship between thermal induced stresses and displacements of non-linearity to a linearized representation.

2.2 Design Approach

Human hands including finger extremities perform rotational movements that are confined to the muscular system, tendons, joints, and bone structure. These rotational movements, specific to a finger, can be generalized from three joints; metacarpophalangeal (MCP), proximal interphalangeal (PIP), and distal interphalangeal (DIP), starting from base to fingertip respectively. Figure 7 is a rendering of finger joints with the values of the length and the minimum/maximum rotational degrees reproduced in Table I. [32] The values below are arbitrary and can be changed for a specific individual based on the amputee's measurements to produce a custom prosthetic. For the purpose of the model developed and analyzed in this study, the values from Xu et. al.[32] experimental finger model will be used in order to provide a base comparison to functional range of rotation to that of the SMA model.

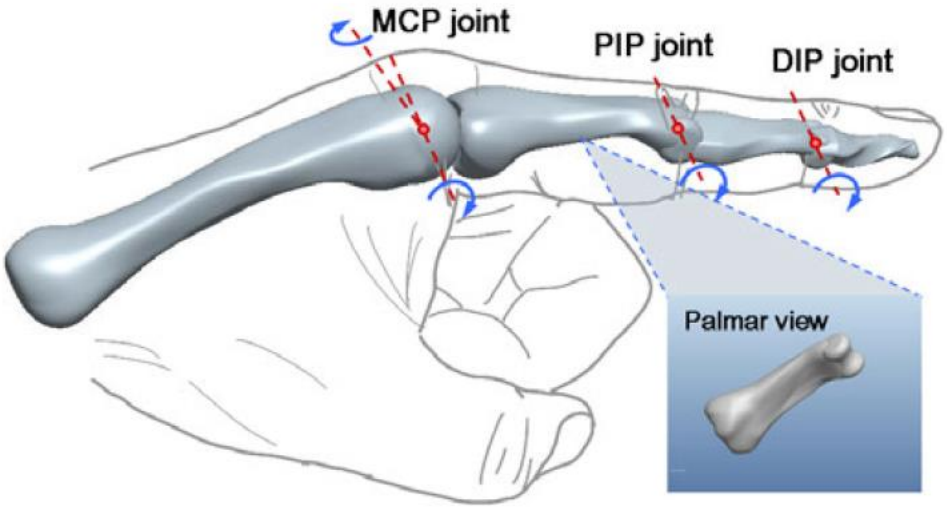

Figure 7: 3D model of the laser-scanned human index finger. Reproduced from Xu *et. al.* [32]

Table I: Physical parameters of the robotic finger skeleton and approximate join motion limits of the robotic finger. Reproduced from Xu *et. al.* [32]

Phalange	*Length (mm)*	*Weight (g)*	*Joint Rotation (θ, degrees)*	
			Minimum	Maximum
MCP** to **PIP	53.4	5.5	30 extension	90 flexion
			35 abduction	35 adduction
PIP** to **DIP	32.0	2.0	0 extension	110 flexion
Distal phalange	23.7	1.2	0 extension	70 flexion

With the objective being reduction of step-like responses in a traditional robotic finger, an SMA slender sheet will be modeled as a single body with a total length of 109 mm. The approach is to define a theorical model of a SMA coupled system, where one SMA is trained in the austenite phase curvature of 90° (close grip) coupled with a martensite phase at 180° (open hand), which will be considered the maximum and minimum displacement boundary conditions, respectively. Utilizing and controlling the hysteresis heat gradient and replacing a multibody system of finger joints, will have a reduced model form of 1-D displacement. For this reason, a maximum range of motion has been applied based on final curvature of the SMA beam. A simplistic and abridged computation expense model will address one-way, (close grip) response time. Future work should resolve the two-way motion of the coupled SMA, open-close hand repetition, along with rate of cooling as proportional to induced strain hardening in opposing SMA. A complete list of material properties used for the analysis of this study is provided in Table II.

Table II: Reference material properties from [33]–[36]

Shape Memory Nitinol 50-55% Ni wt.			
Properties	**Symbol**	**Value**	**Units**
Ambeint Temp	T_∞	23	°C
Austenite Finish	A_f	110	°C
Austenite Start	A_s	80	°C
Austenite Young's Modulus	D_A	75	GPa
Bending Thermal Coeff	Θ	2.71E-04	W/cm-°C
Coeff Themral Expansion	α	6.60E-06	/°C
density	ρ	6.50	g/cm3
Electrical Resistivity	Ω	76.00	µOhm-cm
Elongation	-	10	%
Length	L	10.95	cm
Modulus of Elasticity	E	41.00	GPa
SMA Strain, Initial	ε_0	8	%
Specific Heat	c_p	479.55	J/kg-°C
Thermal Conductivity, Austenite	φ	0.018	W/cm-°C
Thickness	h	0.03	cm
UTS	Y_{UTS}	1070	MPa
Width	b	1.905	cm

3. MODEL DEVELOPMENT

3.1 Heat Transfer of Thermal System

The SMA material heat transfer was applied using electrical resistive heating (joule) and conduction. The thermal resistance is equivalent to electrical resistance, where conservation of charge has the same effect to conservation of heat, and voltage difference similar to temperature difference. [37] Newton's Law of Cooling governs the equation of conduction heat capacitance.

$$P = C\frac{dT}{dt} + \frac{kA}{L}(T - T_{\infty}) \qquad (2)$$

and

$$P = I_{SMA}^2 R \qquad (3)$$

Eqn. (3) is defined with the following values; P is the power source input, I_{SMA}^2 current square ampere of SMA, and R is resistance per length. For Eqn. (2) the first term of the output is $C = mc_p$ the thermal capacitance, with, mass $m = \rho Lbn$, with ρ density, L length, b width and *n*, the height of the SMA beam, and c_p the specific heat. The second term of the sum is characterized as latent heat difference, where the term $\frac{kA}{L}$, is the heat coefficient of conduction. The ambient temperature, T_{∞}, in Eqn. (2) is assumed to be

constant, which removes an added disturbance to the system. [37] The established general equation for heat transfer of conduction is used to find the initial time delay for a uniform linear heat gradient, which is martensite final temperatures to austenite start temperatures, $M_f \rightarrow A_s$. Solving Eqn. (2) and Eqn. (3) numerically, using MATLAB Simulink, gives a time versus temperature response towards A_s temperature. The results in Figure 8, confirm the first step to linearization of input current to temperature rise towards austenite start temperature with respect to time, which is concluded to be approximately 0.65 s. Figure 9 is a free body diagram illustrating $M_f \rightarrow A_s$ linear region of no phase transformation. The second region undergoes a phase transformation of $A_s \rightarrow A_f$ temperatures, which provides the dynamic response of the SMA component under heating. The pre-trained SMA for this model makes the assumption that the transformation of heating in austenite final temperature, A_f will also be the beam completed displacement in 1-D direction.

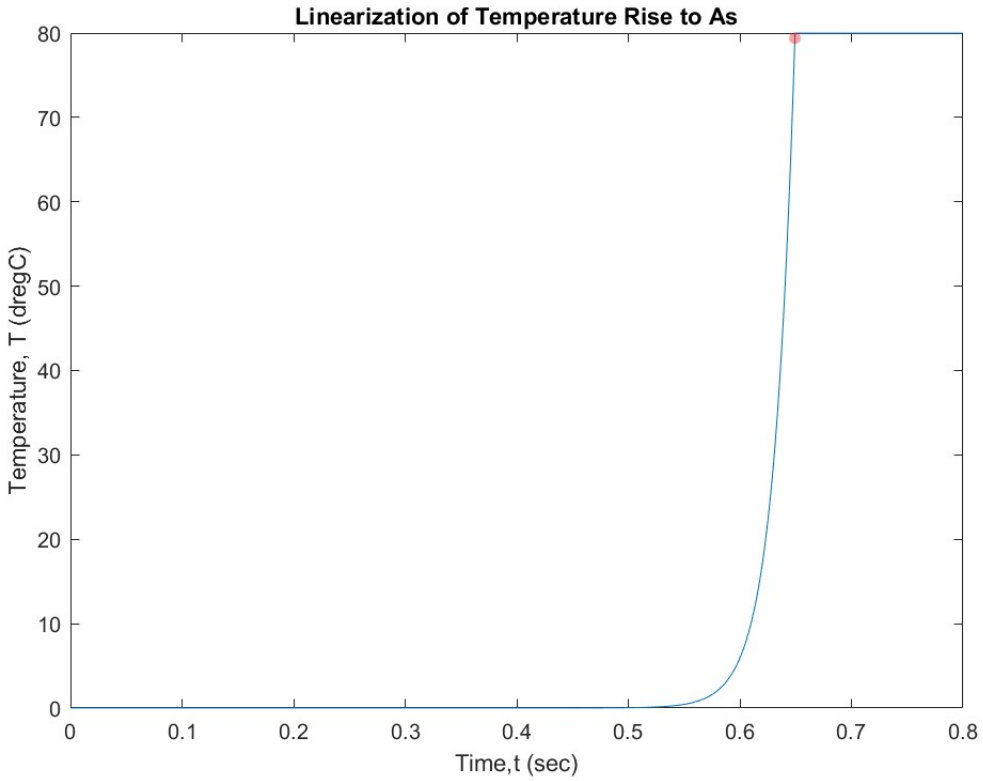

Figure 8: Linearization of input current as a response to temperature rise verse time, initializing time response of $M_f \rightarrow A_s$. Reference Appendix A.

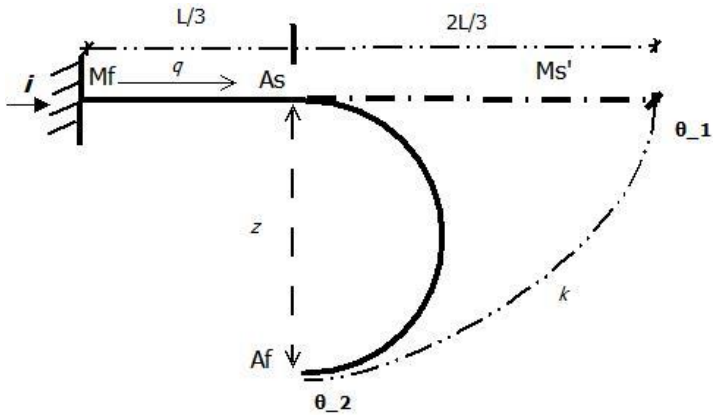

Figure 9: Free body diagram of SMA finger in the form of a cantilever beam in 1-D and final displacement from $M_f \rightarrow A_s$, and $A_s \rightarrow A_f$.

3.2 Phase Transformation and Constitutive Model

The modeled equations that govern the phenomenon of SME are described in various research material, all of which, are focused on the volume fraction of martensite and the thermal change characteristics with respect to the heat medium. The challenge is such that, SMAs non-linear properties combined with phase transformation, stress applied, and heat differences, are a few variables that drive complex equations in solving the shape memory effect. In general, materials have impurities associated with manufacturing capabilities that limit these equations to the actual physical attributes of the material. For this reason, most analyses are performed with both numerical systems and physical experiments to evaluate the difference in error. The approach defined in this study focuses on the phase transformation model of the volume fraction coefficient to the

linear region of heating only. Starting with Brinson and Tanaka's phase transformation model equation for heating:

$$\xi = \frac{-\xi_m}{2}\cos[a_A(T - A_s) + b_A\sigma] + 1 \qquad (4)$$

where, ξ_m is the volume fraction of martensite, SMA temperature *T*, austenite phase temperature starts A_s, $a_A = \frac{\pi}{A_f - A_s}$, $b_A = -a_A/C_A$, where C_A is a curve fitting parameter constant, and stress tensor σ . Including a time derivative for Eqn. (4) yields the state equation during heating for volume fraction rate: Eqn. (5).

$$\dot{\xi} = \frac{-\xi_m}{2}\sin[a_A(T - A_s) + b_A\sigma]\left[b_A\dot{T} + b_A\dot{\sigma}\right] \qquad (5)$$

The driving force to form a given martensite fraction can be approximated by extrapolating the temperature rise from $A_s \rightarrow A_f$ with respect to $\sigma_L \rightarrow \sigma_H$ over time. Figure 10 illustrates a linearized model of the hysteresis loop, which displays the lower boundary of $A_s \rightarrow A_f$ temperatures regions ($a \rightarrow b \rightarrow i$). An approximation of this region was performed using algebraic methods with Pythagorean theorem of a parallelogram to linearized the martensite volume fraction coefficient.

$$\dot{\xi} = -\frac{\xi}{2} + \frac{\sigma}{A_D} + \dot{T}R \qquad (6)$$

Where, $A_D = A_f - A_s$ and R is the resistance per unit length, which is proportional to rate of temperature change, $\dot{T}$.

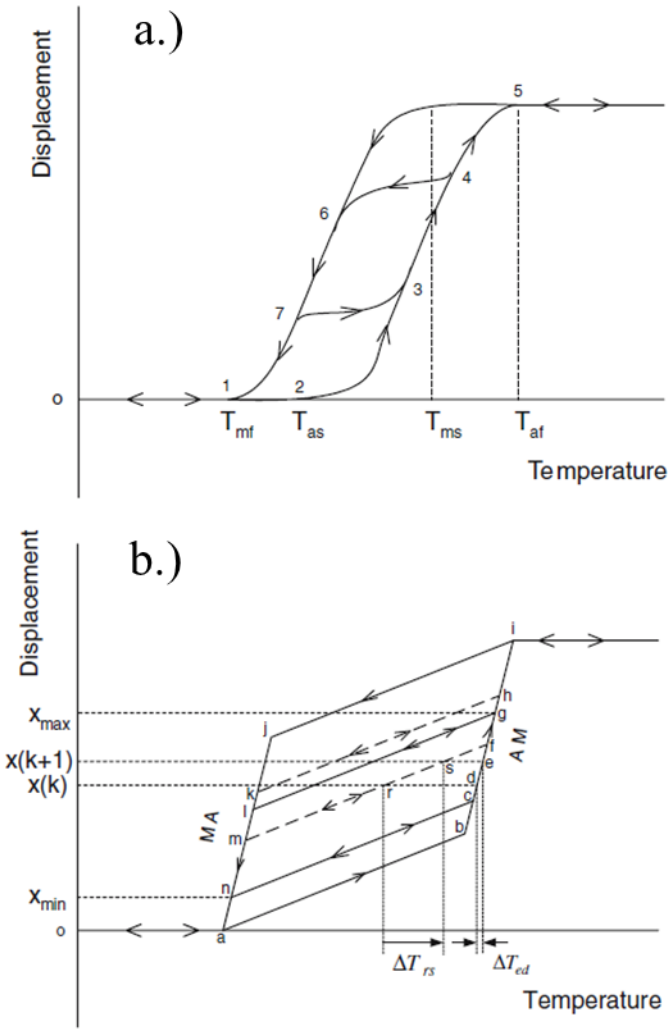

Figure 10: Graph a.) typical SMA hysteresis loop and b.) a linear approximation. Reproduced from Kumagai *et. al.* [38]

The convolution method for solution of Gibbs free energy equation, along with thermomechanical transformation hardening formulation derives the second feature of SMA models; the constitutive law. Lagoudas *et. al.* states that the magnitude of the inelastic recoverable strain is the same for all transformations under an applied stress level and their approach is to consider a non-linear analytical relation between the magnitude of the transformation strain rate ($\dot{\varepsilon}$) and the applied stress rate ($\dot{\sigma}$). [39] Since the work in this study will focus on 1-D thermomechanical constitutive relation of the SMA a version including the rate of temperature ($\dot{T}$) from Liang et. al and previously, Lagoudas et. al, will be used in the form [34], [40]:

$$\dot{\sigma} = D\dot{\varepsilon} + \alpha\dot{T} + \Omega\dot{\xi} \qquad (7)$$

where $D = \frac{D_M + D_A}{2}$, is the average Young's modulus of D_M martensite and D_A austenite, respectively and α is the thermal expansion coefficient, and $\Omega = -\mathrm{D}\varepsilon_0$. The study adopts the assumption of phase transformation in heating only of $A_s \rightarrow A_f$ region, therefore in Eqn. (7), D will be equal to D_A.

3.3 Dynamics Model

The mechanical analysis of a cantilever beam takes the fundamentals of an applied force and reaction called a moment arm in obtaining stress-strain relationship, displacements, torsion, and other mechanical responses. An SMA finger designed in this analysis, being one-dimensional, reduces the stress and strain from three-dimensions typically evaluated in beam calculations, further simplifying the rotational displacement of the action associated with close grip hand motion. Tuzcu *et. al.* [41] explored a sophisticated numerically derived analysis of vibration control in a thermoelastic beam using heat actuation, which associated the internal heat conduction of the beam to the dynamic control system of vibration dampening. Although the beam was controllable, theoretically their analysis applied external heat convection and force. Elahinia and Ashrafiuon [35] utilized Variable Structure Control (VSC), in a PID control system of a SMA actuated manipulator. The moment arm manipulator was actuated via a SMA spring-mass-damper system with a bias spring and end load which provide the opposing work of the SMA under phase transformation through means of electrical-mechanic (thermal) input. The following equation uses a linearized modifications to accompany the overall dynamic cantilever beam model.

$$I\ddot{\theta} = \frac{2}{3}Lg\theta - E\alpha\dot{\theta} + \frac{2}{3}L^2bh\sigma \qquad (8)$$

Where $I\ddot{\theta}$ is the equivalent mass moment of inertias, g is the gravity coefficient, $E\alpha\dot{\theta}$ is the thermal bending coefficient, and the last term of Eqn. (8) references a volume per

meter-force change in a cross-sectional area, leaving a moment arm [N-m] unit of measure. Per, L. Euler-Bernoulli [41], beam theory of longitudinal elastic displacement over the thickness of the beam, it can be assumed that the beam is slender; twice the thickness, *2h*, width *b*, and much longer then their length, *L*, gives Eqn. (9) for inertia, *I*:

$$I = b\int_{-h}^{h} y^2 dy = \frac{2}{3}bh^3 \qquad (9)$$

4. RESULTS

4.1 Numerical Analysis

The modeled analysis developed in this study compiled heat transfer, phase transformations, constitutive law and kinematics equations in order to implement a non-load bearing force of actuation via joules heating. In order to perform a multiple input-multiple output (MIMO) system, a state space set of equations were established in the form of a matrix argument state model.

$$\dot{\mathbf{x}} = \mathbf{Ax} + \mathbf{Bu} \qquad (10)$$

$$\mathbf{y} = \mathbf{Cx} + \mathbf{Du} \qquad (11)$$

where **x** is the vector of state variables, **u** is the vector of input functions, and **y** is the vector of output variables. The state variable matrix arguments creates a Linear Time Invariant (LTI) system to solve MIMO parameters.[37] Formulating the equations for phase transformation (Eqn. (6)), heat transfer (Eqn. (2)) and dynamics (Eqn. (8)) into the constitutive law (Eqn. (7)), resulted in a system of first order differential equations (ODE) in state variable form (Eqn. (10)) and the input function (Eqn. (11)) corresponds to input values of Eqn. (3). Appendix A, provides the numerically derived transfer functions and matrix arguments demonstrated with MATLAB Simulink Toolbox of the state space variables displayed in Figure 11. Each open loop system runs the LTI matrices of Eqn. (10) and (11), to solve a continuous-time state space model. The amplified gain value, *K*, was chosen from root-locus values provided by the Linear

Analyzer tool in Simulink, thus forming two simplified closed-loop systems to solve for displacement, θ, and temperature, T. Additionally, the Saturation Block for each closed-looped system, confines the output conditions within the boundary defined of temperature and position, for this case 80-110°C and sine(90°) respectively.

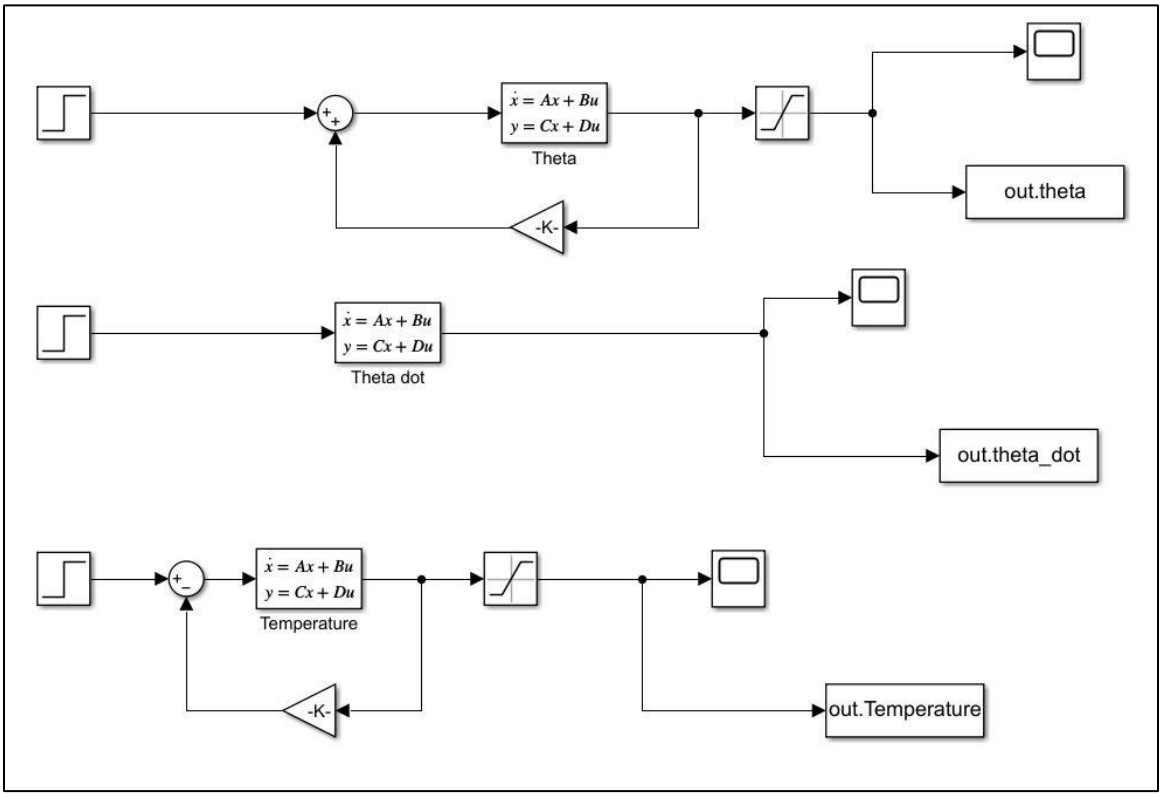

Figure 11: Displaying Simulink Workspace of three LTI State-space variable open-loop systems. Top; displacement, θ approaching 90°, Middle; angular velocity, $\dot{\theta}$, Bottom; temperature, T

4.2 Displacement vs Time

In Figure 9, a final curvature, k (close grip) for the trained SMA beam has a maximum displacement from θ_1 and θ_2 as final angle of $\theta_f = 90°$. The MATLAB Simulink computational results of displacement over time reached θ_f in approximately 1.03 s including the martensite to austenite phase transformation of approximately 0.65 s. Figure 12, concludes the output graphed region of the maximum rotation for $2/3L$ as $A_s \rightarrow A_f$ approaches θ_f , where $\sin(\theta) = 1$. The input step response voltage continues with the time duration of the MATLAB simulation holding at θ_f.

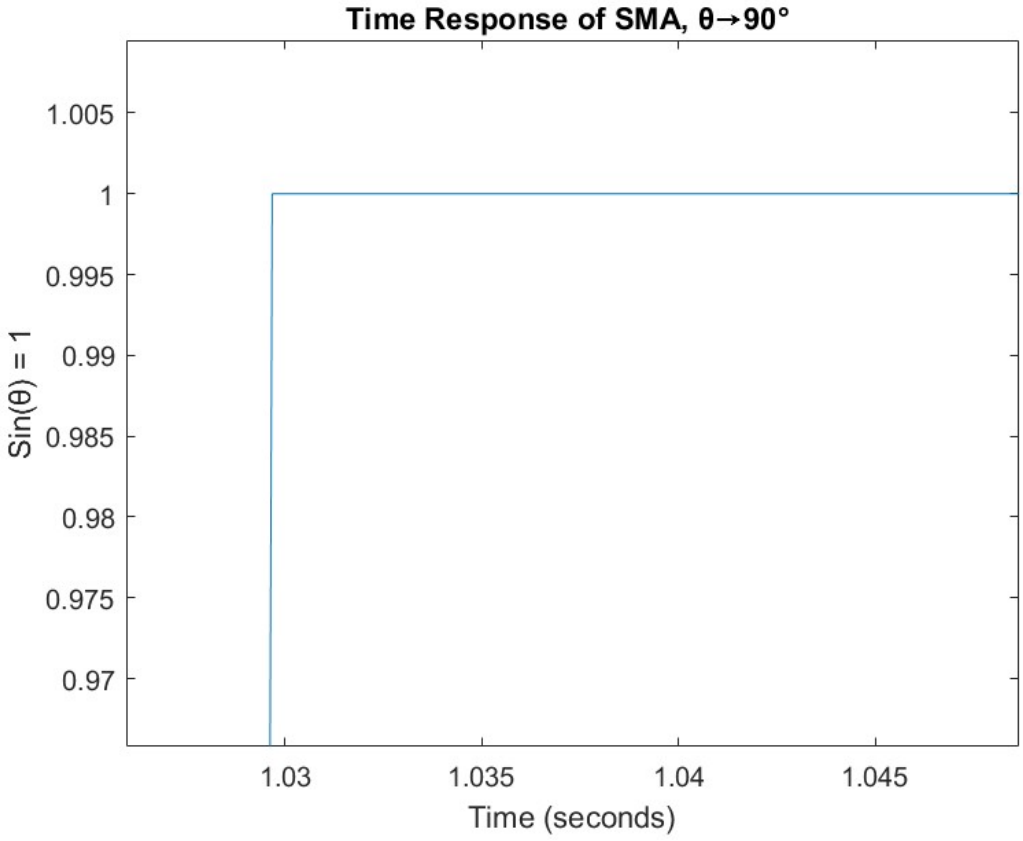

Figure 12: Time vs. Displacement, θ, approaching final angle, θ_f of the theoretically trained SMA from neutral axis, ~1.03s.

5. DISCUSSION

This study exhibits exploration of an alternative to traditional robotic prosthetics that can, theoretically, improve the time response from an input EMG signal with the use of a SMA structure. Future works should be considered, as this study contributed a small portion to a greater complex system towards SMAs in an application of hand robotics. In utilization of EMG processing inputs, additional and multiple methods should be considered when identifying EMG information to physical reactions in 3-D responses such as; artificial neural networks (ANN), Bayesian classifier (BC), fuzzy logic (FL), multilayer perceptron (MLP), support vector machines (SVM), linear discriminant analysis (LDA), hidden Markov models (HMM) and K-nearest neighbor (KNN) method.[24] Implementing a complex close-loop analysis, schematic in Figure 13, characterizes the heating and cooling affect in complete reversable phase transformation. A physical experiment as proof of concept to compare a complex model in Figure 13, would also represent rate of work reversal with an applied opposite SMA coupler. Part of this objective would show the peak bending influences on cooling rate as displacement of the material is reaching martensite phase. Because the SMA coupled system would need an additional buffer layer, research should include a semiconductor material, such as polymer elastomer.[42] The radius of curvature as a function of temperature can be a non-monotonic function (NMF), different material experiments to solve NMF should be explored. For example Figure 14, Halbert, shows two different sets of material properties where the folding angle behaved differently on reverse transformation. [43]

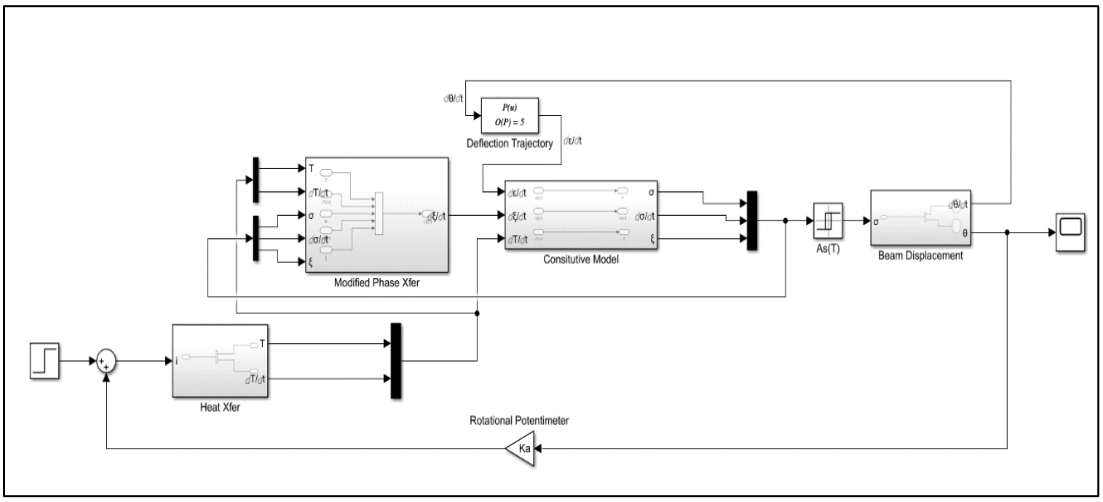

Figure 13: Simulink control system schematic of SMA input current to output displacement and angular velocity.

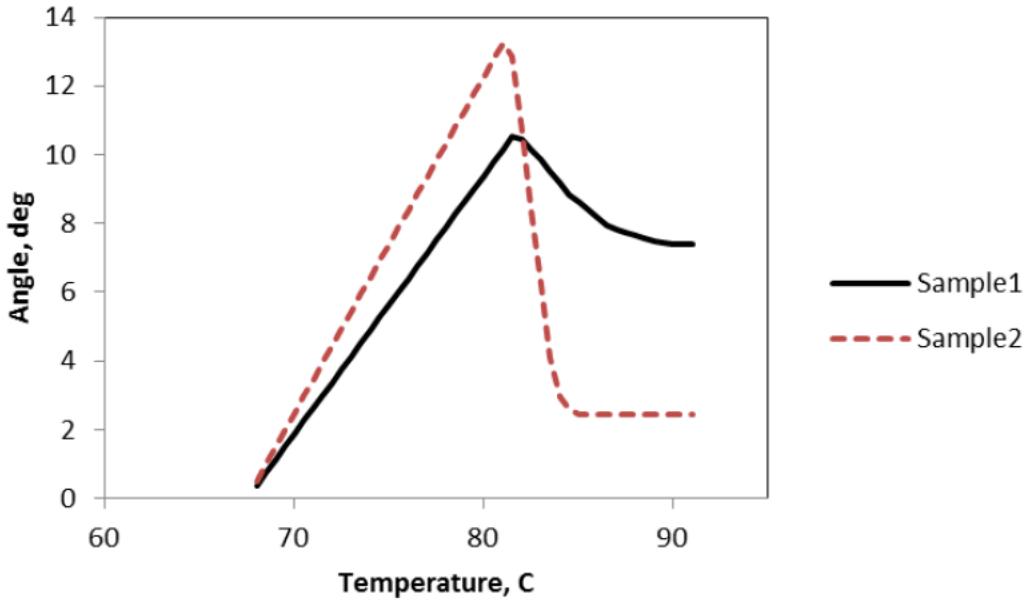

Figure 14: Fold angle for two different sets of material properties during heating of SMAs. Reproduced from Halber *et. al.* [43]

6. CONCLUSION

In conclusion, the work in this study developed a proof of concept for an SMA model in solving the problem of slow time responses for traditional robotic hand movements. The method of numerical analysis provided validation of a solution in the use of SMA material for a finger in close grip response. Impact of this work is a small contribution in advancing bionics of human-like functionality in prosthetics. The proposed use of SMAs in the form of a coupling push-pull system through thermoelectric (joules heating) actuation, has provided an early-stage solution to traditional electric servo-motor-drive systems currently used in a robotic hand. The focus is on a single extremity finger, restricted to one-dimensional reduction, producing a simplified model. In the numerical analysis, the theoretical results demonstrated roughly 1.03 s or 46% faster in close grip function to that of a robotic finger at 2.25 s. MATLAB Simulink, the program utilized to develop a numerical model resulting in comparative analysis between the SMA hysteresis heat gradient control response and displacement, has been produced. The analysis developed can be multiplied into a full human hand analysis in future work. Defined variables of material properties, thermal gradient threshold, and electrothermal inputs have been concluded in this theoretical modeled solution.

APPENDIX A: MATLAB CODE FOR LTI OPEN-LOOP

```
%Martensite to Austenite LTI
sysMs =
                158.7
 ------------------------------------------------
 5.715e-05 s^4 - 0.001314 s^3 + 1951 s^2 + 6.858 s
Continuous-time transfer function.
>> sysPWR=tf(Pwr_input)
sysPWR =
    1
 ------
 76 s^3
Continuous-time transfer function.
%State-space model of X_dot = Ax+Bu and y=Cx+Du
>> sys=ss(A_m, B_m, C_m, D_m)
sys =
  A =
          x1         x2         x3         x4         x5
  x1         0          1          0          0          0
  x2  -2.088e+08      -7.892          0   1.217e+04          0
  x3         0          0  -7.224e-08          0          0
  x4         0         75   4.335e-07       -0.2          3
  x5         0          0   -5.49e-06    0.03333       -0.5
  B =
```

```
          u1
  x1       0
  x2       0
  x3  0.004641
  x4  0.004641
  x5  0.004641


 C =
      x1  x2  x3  x4  x5
  y1   1   0   0   0   0
  y2   0   1   0   0   0


 D =
      u1
  y1   0
  y2   0


Continuous-time state-space model.
> sys1=tf(sys)
sys1 =
  From input to output...
                    56.46 s^2 + 197.6 s - 0.0009034
  1:  ------------------------------------------------------------------
      s^5 + 8.592 s^4 + 2.079e08 s^3 + 1.457e08 s^2 + 10.52 s + 6.543e-17


              56.46 s^3 + 197.6 s^2 - 0.0009034 s + 2.48e-18
```

```
  2:  ------------------------------------------------------------------

      s^5 + 8.592 s^4 + 2.079e08 s^3 + 1.457e08 s^2 + 10.52 s + 6.543e-17

%Theta = Displacement

sys2=tf(sys_theta)

sys2 =

                  56.46 s^2 + 197.6 s - 0.0009034

 ------------------------------------------------------------------------

 s^5 + 8.592 s^4 + 2.079e08 s^3 + 1.457e08 s^2 + 10.52 s + 6.543e-17

 Continuous-time transfer function.

%Theta_dot is the velocity of displacement

sys3=tf(sys_theta_dot)

sys3 =

           56.46 s^3 + 197.6 s^2 - 0.0009034 s + 7.539e-19

 ------------------------------------------------------------------------

 s^5 + 8.592 s^4 + 2.079e08 s^3 + 1.457e08 s^2 + 10.52 s + 6.543e-17


Continuous-time transfer function.

%Temperature Gradient of As to Af

sys2=tf(sys_temp)

sys2 =

    0.004641

 ------------

 s + 7.224e-08

 Continuous-time transfer function.
```

```
>> whos
  Name            Size          Bytes  Class                Attributes
  A_f             1x1               8  double
  A_m             5x5             200  double
  A_s             1x1               8  double
  Ad              1x1               8  double
  Area            1x1               8  double
  B_m             5x1              40  double
  C               1x1               8  double
  C_m             2x5              80  double
  C_temp          1x5              40  double
  C_theta         1x5              40  double
  C_theta_dot     1x5              40  double
  Cb              1x1               8  double
  Cp              1x1               8  double
  DA              1x1               8  double
  D_1             1x1               8  double
  D_m             2x1              16  double
  E               1x1               8  double
  G_amp           1x1               8  double
  Heat_transfer   1x1            1329  tf
  I               1x1               8  double
  L               1x1               8  double
  L_A             1x1               8  double
```

Ohms	1x1	8	double
P	1x1	8	double
Pc	1x1	8	double
Pwr_input	1x1	1313	tf
R	1x1	8	double
Tamb	1x1	8	double
V_a	1x1	8	double
a1	1x1	8	double
a10	1x1	8	double
a11	1x1	8	double
a2	1x1	8	double
a4	1x1	8	double
a5	1x1	8	double
a6	1x1	8	double
a7	1x1	8	double
a8	1x1	8	double
a9	1x1	8	double
a_f	1x1	8	double
alpha	1x1	8	double
ans	0x0	0	double
b	1x1	8	double
c1	1x1	8	double
c2	1x1	8	double
d	1x1	8	double
g	1x1	8	double
h	1x1	8	double

h0	1x1	8	double
h2	1x1	8	double
ka_ht	1x1	8	double
kc	1x1	8	double
out	1x1	21975	Simulink.SimulationOutput
q1	1x1	8	double
q2	1x1	8	double
r	1x1	8	double
s	1x1	1281	tf
strain_int	1x1	8	double
sys	2x1	1666	ss
sys1	2x1	1665	tf
sys2	1x1	1281	tf
sys3	1x1	1345	tf
sys_temp	1x1	1610	ss
sys_theta	1x1	1610	ss
sys_theta_dot	1x1	1610	ss
volts	1x1	8	double

APPENDIX B: ELECTRICAL PARAMETERS

Volts[1] (V)	Resistance[1] (Ω)	Power (W) (v2/r)	Pwr Amplified (W)' (7x)	Volts (V)'
5.0	50.8	0.49213	3.44488	13.22876
6.0	50.8	0.70866	4.96063	15.87451
7.0	50.8	0.96457	6.75197	18.52026
7.2	50.8	1.02047	7.14331	19.04941
7.4	50.8	1.07795	7.54567	19.57856
7.5	50.8	1.10728	7.75098	19.84313
7.6	50.8	1.13701	7.95906	20.10771
7.7	50.8	1.16713	8.16988	20.37229
7.8	50.8	1.19764	8.38346	20.63686
8.0	50.8	1.25984	8.81890	21.16601
8.1	50.8	1.29154	9.04075	21.43059

[1] M. H. Elahinia and H. Ashrafiuon, "Nonlinear Control of a Shape Memory Alloy Actuated Manipulator," *J. Vib. Acoust.*, vol. 124, no. 4, pp. 566–575, Oct. 2002, doi: 10.1115/1.1501285.

New Resistance[2] (Ω)	Current (i)	Current Amplified (i)'	Power (W) (i2r)'	Volts(SMA) (V)'
76.0	0.08047	0.21290	3.44488	16.18058
76.0	0.09656	0.25548	4.96063	19.41669
76.0	0.11266	0.29806	6.75197	22.65281
76.0	0.11588	0.30658	7.14331	23.30003
76.0	0.11909	0.31510	7.54567	23.94725
76.0	0.12070	0.31935	7.75098	24.27086
76.0	0.12231	0.32361	7.95906	24.59447
76.0	0.12392	0.32787	8.16988	24.91809
76.0	0.12553	0.33213	8.38346	25.24170
76.0	0.12875	0.34064	8.81890	25.88892
76.0	0.13036	0.34490	9.04075	26.21253

[2] sabinek, "Nitinol Products & Frames," *Confluent Medical*. https://confluentmedical.com/capabilities/nitinol-component-manufacturing/ (accessed Nov. 13, 2022).

REFERENCES

[1] P. Wattanasiri, P. Tangpornprasert, and C. Virulsri, "Design of Multi-Grip Patterns Prosthetic Hand with Single Actuator," *IEEE Trans. Neural Syst. Rehabil. Eng.*, pp. 1–1, 2018, doi: 10.1109/TNSRE.2018.2829152.

[2] T. W. Duerig, K. N. Melton, and D. Stöckel, *Engineering aspects of shape memory alloys*. Butterworth-heinemann, 2013.

[3] W. J. Moberly, *Mechanical twinning and twinless martensite in ternary titanium (50) nickel (50-x) M (x) intermetallics*. Stanford university, 1991.

[4] K. Otsuka and K. Shimizu, "Morphology and crystallography of thermoelastic Cu–Al–Ni martensite analyzed by the phenomenological theory," *Trans. Jpn. Inst. Met.*, vol. 15, no. 2, pp. 103–108, 1974.

[5] M. A. Meyers and K. K. Chawla, *Mechanical behavior of materials*. Cambridge university press, 2008.

[6] W. J. Buehler, J. V. Gilfrich, and R. C. Wiley, "Effect of low-temperature phase changes on the mechanical properties of alloys near composition TiNi," *J. Appl. Phys.*, vol. 34, no. 5, pp. 1475–1477, 1963.

[7] W. Tang, B. Sundman, R. Sandström, and C. Qiu, "New modelling of the B2 phase and its associated martensitic transformation in the Ti–Ni system," *Acta Mater.*, vol. 47, no. 12, pp. 3457–3468, Sep. 1999, doi: 10.1016/S1359-6454(99)00193-7.

[8] J. Frenzel, E. P. George, A. Dlouhy, Ch. Somsen, M. F.-X. Wagner, and G. Eggeler, "Influence of Ni on martensitic phase transformations in NiTi shape memory alloys," *Acta Mater.*, vol. 58, no. 9, pp. 3444–3458, May 2010, doi: 10.1016/j.actamat.2010.02.019.

[9] A. M. Pérez-Sierra, J. Pons, R. Santamarta, I. Karaman, and R. D. Noebe, "Stability of a Ni-rich Ni-Ti-Zr high temperature shape memory alloy upon low temperature aging and thermal cycling," *Scr. Mater.*, vol. 124, pp. 47–50, Nov. 2016, doi: 10.1016/j.scriptamat.2016.06.029.

[10] T. Ezaz, J. Wang, H. Sehitoglu, and H. J. Maier, "Plastic deformation of NiTi shape memory alloys," *Acta Mater.*, vol. 61, no. 1, pp. 67–78, Jan. 2013, doi: 10.1016/j.actamat.2012.09.023.

[11] V. P. Iasnii and R. Junga, "Phase Transformations and Mechanical Properties of the Nitinol Alloy with Shape Memory," *Mater. Sci.*, vol. 54, no. 3, pp. 406–411, Nov. 2018, doi: 10.1007/s11003-018-0199-7.

[12] T. W. Duerig, "Some unsolved aspects of Nitinol," *Mater. Sci. Eng. A*, vol. 438–440, pp. 69–74, Nov. 2006, doi: 10.1016/j.msea.2006.05.072.

[13] O. Akgul, H. O. Tugrul, and B. Kockar, "Effect of the cooling rate on the thermal and thermomechanical behavior of NiTiHf high-temperature shape memory alloy," *J. Mater. Res.*, vol. 35, no. 12, pp. 1572–1581, Jun. 2020, doi: 10.1557/jmr.2020.139.

[14] L. Resnik, S. L. Klinger, and K. Etter, “The DEKA Arm: Its features, functionality, and evolution during the Veterans Affairs Study to optimize the DEKA Arm,” *Prosthet. Orthot. Int.*, vol. 38, no. 6, pp. 492–504, Dec. 2014, doi: 10.1177/0309364613506913.

[15] “Dean Kamen | Biography, Segway, & Facts | Britannica.” https://www.britannica.com/biography/Dean-Kamen (accessed Nov. 25, 2022).

[16] “The LUKE/DEKA advanced prosthetic arm.” https://www.research.va.gov/research_in_action/The-LUKE-DEKA-advanced-prosthetic-arm.cfm (accessed Nov. 25, 2022).

[17] C. Della Santina, G. Grioli, M. Catalano, A. Brando, and A. Bicchi, “Dexterity augmentation on a synergistic hand: The Pisa/IIT SoftHand+,” in *2015 IEEE-RAS 15th International Conference on Humanoid Robots (Humanoids)*, Seoul, Nov. 2015, pp. 497–503. doi: 10.1109/HUMANOIDS.2015.7363595.

[18] C. D. Santina, C. Piazza, G. Grioli, M. G. Catalano, and A. Bicchi, “Toward Dexterous Manipulation With Augmented Adaptive Synergies: The Pisa/IIT SoftHand 2,” *IEEE Trans. Robot.*, vol. 34, no. 5, pp. 1141–1156, Oct. 2018, doi: 10.1109/TRO.2018.2830407.

[19] “Michelangelo hand | The Michelangelo hand helps you regain extensive freedom.” https://www.ottobock.com/en-us/product/8E500 (accessed Nov. 13, 2022).

[20] S. Mayer, G. O’Dell, and Y. B. Sipka, “Dexter: A Smart Prosthetic Device for Transradial Amputees,” p. 76.

[21] Zhe Xu and E. Todorov, “Design of a highly biomimetic anthropomorphic robotic hand towards artificial limb regeneration,” in *2016 IEEE International Conference on Robotics and Automation (ICRA)*, Stockholm, Sweden, May 2016, pp. 3485–3492. doi: 10.1109/ICRA.2016.7487528.

[22] P. Parker, K. Englehart, and B. Hudgins, “Myoelectric signal processing for control of powered limb prostheses,” *J. Electromyogr. Kinesiol.*, vol. 16, no. 6, pp. 541–548, Dec. 2006, doi: 10.1016/j.jelekin.2006.08.006.

[23] S. Bhagwat and P. Mukherji, “Electromyogram (EMG) based fingers movement recognition using sparse filtering of wavelet packet coefficients,” *Sādhanā*, vol. 45, no. 1, p. 3, Dec. 2020, doi: 10.1007/s12046-019-1231-9.

[24] E. F. Shair, N. A. Jamaluddin, and A. R. Abdullah, “Finger Movement Discrimination of EMG Signals Towards Improved Prosthetic Control using TFD,” *Int. J. Adv. Comput. Sci. Appl.*, vol. 11, no. 9, 2020, doi: 10.14569/IJACSA.2020.0110928.

[25] C. J. De Luca, “Physiology and Mathematics of Myoelectric Signals,” *IEEE Trans. Biomed. Eng.*, vol. BME-26, no. 6, pp. 313–325, Jun. 1979, doi: 10.1109/TBME.1979.326534.

[26] N. Araki, K. Inaya, Y. Konishi, and K. Mabuchi, “An artificial finger robot motion control based on finger joint angle estimation from EMG signals for a robot prosthetic hand system,” p. 3.

[27] P. P. Vu *et al.*, "A regenerative peripheral nerve interface allows real-time control of an artificial hand in upper limb amputees," *Sci. Transl. Med.*, vol. 12, no. 533, p. eaay2857, Mar. 2020, doi: 10.1126/scitranslmed.aay2857.

[28] F. Preisach, "Über die magnetische Nachwirkung," *Z. Für Phys.*, vol. 94, pp. 277–302, 1935.

[29] L. C. Brinson, A. Bekker, and S. Hwang, "Deformation of Shape Memory Alloys Due to Thermo-Induced Transformation," *J. Intell. Mater. Syst. Struct.*, vol. 7, no. 1, pp. 97–107, Jan. 1996, doi: 10.1177/1045389X9600700111.

[30] K. Tanaka and S. Nagaki, "A thermomechanical description of materials with internal variables in the process of phase transitions," *Ing.-Arch.*, vol. 51, no. 5, pp. 287–299, 1982, doi: 10.1007/BF00536655.

[31] S. Majima, K. Kodama, and T. Hasegawa, "Modeling of shape memory alloy actuator and tracking control system with the model," *IEEE Trans. Control Syst. Technol.*, vol. 9, no. 1, pp. 54–59, Jan. 2001, doi: 10.1109/87.896745.

[32] Z. Xu, V. Kumar, Y. Matsuoka, and E. Todorov, "Design of an anthropomorphic robotic finger system with biomimetic artificial joints," in *2012 4th IEEE RAS & EMBS International Conference on Biomedical Robotics and Biomechatronics (BioRob)*, Rome, Italy, Jun. 2012, pp. 568–574. doi: 10.1109/BioRob.2012.6290710.

[33] sabinek, "Nitinol Products & Frames," *Confluent Medical*. https://confluentmedical.com/capabilities/nitinol-component-manufacturing/ (accessed Dec. 13, 2022).

[34] C. Liang and C. A. Rogers, “One-dimensional thermomechanical constitutive relations for shape memory materials,” *J. Intell. Mater. Syst. Struct.*, vol. 8, no. 4, pp. 285–302, 1997.

[35] M. H. Elahinia and H. Ashrafiuon, “Nonlinear Control of a Shape Memory Alloy Actuated Manipulator,” *J. Vib. Acoust.*, vol. 124, no. 4, pp. 566–575, Oct. 2002, doi: 10.1115/1.1501285.

[36] T. Waram, *Actuator design using shape memory alloys*. Hamilton, Ont.: TC Waram, 1993.

[37] W. J. Palm III, *System Dynamics*, 4th Edition. Universtiy of Rhode Island: McGraw-Hill Education, 2021.

[38] A. Kumagai, T.-I. Liu, and P. Hozian, “Control of Shape Memory Alloy Actuators with a Neuro-fuzzy Feedforward Model Element,” *J. Intell. Manuf.*, vol. 17, no. 1, pp. 45–56, Feb. 2006, doi: 10.1007/s10845-005-5512-2.

[39] D. Lagoudas, D. Hartl, Y. Chemisky, L. Machado, and P. Popov, “Constitutive model for the numerical analysis of phase transformation in polycrystalline shape memory alloys,” *Int. J. Plast.*, vol. 32–33, pp. 155–183, May 2012, doi: 10.1016/j.ijplas.2011.10.009.

[40] Z. Ding and D. C. Lagoudas, “Transient heat transfer behavior of one-dimensional symmetric thermoelectric SMA actuators,” *Math. Comput. Model.*, vol. 29, no. 1, pp. 33–55, Jan. 1999, doi: 10.1016/S0895-7177(98)00177-0.

[41] I. Tuzcu, J. K. Moua, and J. G. Olivares, “Control of a thermoelastic beam using heat actuation,” *J. Vib. Control*, p. 1077546316629251, 2016.

[42] T. Mirfakhrai, J. D. W. Madden, and R. H. Baughman, “Polymer artificial muscles,” *Mater. Today*, vol. 10, no. 4, pp. 30–38, Apr. 2007, doi: 10.1016/S1369-7021(07)70048-2.

[43] T. Halbert, P. Moghadas, R. Malak, and D. Hartl, “Control of a Shape Memory Alloy Based Self-Folding Sheet,” in *Volume 5B: 38th Mechanisms and Robotics Conference*, Buffalo, New York, USA, Aug. 2014, p. V05BT08A041. doi: 10.1115/DETC2014-34703.

ProQuest Number: 30244404

INFORMATION TO ALL USERS
The quality and completeness of this reproduction is dependent on the quality
and completeness of the copy made available to ProQuest.

Distributed by ProQuest LLC (2023).
Copyright of the Dissertation is held by the Author unless otherwise noted.

This work may be used in accordance with the terms of the Creative Commons license
or other rights statement, as indicated in the copyright statement or in the metadata
associated with this work. Unless otherwise specified in the copyright statement
or the metadata, all rights are reserved by the copyright holder.

This work is protected against unauthorized copying under Title 17,
United States Code and other applicable copyright laws.

Microform Edition where available © ProQuest LLC. No reproduction or digitization
of the Microform Edition is authorized without permission of ProQuest LLC.

ProQuest LLC
789 East Eisenhower Parkway
P.O. Box 1346
Ann Arbor, MI 48106 - 1346 USA